SANDIA REPORT

SAND99–1104
Unlimited Release
Printed June 1999

Modeling of Oblique Penetration into Geologic Targets Using Cavity Expansion Penetrator Loading with Target Free-Surface Effects

Donald B. Longcope, Jr., Mazen R. Tabbara, and Joe Jung

Prepared by
Sandia National Laboratories
Albuquerque, New Mexico 87185 and Livermore, California 94550

Sandia is a multiprogram laboratory operated by Sandia Corporation, a Lockheed Martin Company, for the United States Department of Energy under Contract DE-AC04-94AL85000.

Sandia National Laboratories

Issued by Sandia National Laboratories, operated for the United States Department of Energy by Sandia Corporation.

Available to DOE and DOE contractors from
Office of Scientific and Technical Information
P.O. Box 62
Oak Ridge, TN 37831

Prices available from (703) 605-6000
Web site: http://www.ntis.gov/ordering.htm

Available to the public from
National Technical Information Service
U.S. Department of Commerce
5285 Port Royal Rd
Springfield, VA 22161

NTIS price codes
Printed copy: A03
Microfiche copy: A01

DISCLAIMER

Portions of this document may be illegible in electronic image products. Images are produced from the best available original document.

SAND99-1104
Unlimited Release
Printed June 1999

Modeling of Oblique Penetration into Geologic Targets Using Cavity Expansion Penetrator Loading with Target Free-Surface Effects

Donald B. Longcope, Jr.
Structural Dynamics and Vibration Control Department

Mazen R. Tabbara
Joe Jung
Engineering and Manufacturing Mechanics

Sandia National Laboratories
P.O. Box 5800
Albuquerque, NM 87185-0439

Abstract

A procedure has been developed to represent the loading on a penetrator and its motion during oblique penetration into geologic media. The penetrator is modeled with the explicit dynamics, finite element computer program PRONTO 3D and the coupled pressure on the penetrator is given in a new loading option based on a separate cavity expansion (CE) solution that accounts for the pressure reduction from a nearby target free surface. The free-surface influence distance is selected in a predictive manner by considering the pressure to expand a spherical cavity in a finite radius sphere of the target material. The CE/PRONTO 3D procedure allows a detailed description of the penetrator for predicting shock environments or structural failure during the entire penetration event and is sufficiently rapid to be used in design optimization. It has been evaluated by comparing its results with data from two field tests of a full-scale penetrator into frozen soil at an impact angles of 49.6 and 52.5 degrees from the horizontal. The measured penetrator rotations were 24 and 22 degrees, respectively. In the simulation, the rotation was 21 degrees and predominately resulted from the pressure reduction of the free surface. Good agreement was also found for the penetration depth and axial and lateral acceleration at two locations in the penetrator.

Acknowledgements

The authors would like to thank Tom Warren for helpful interaction on the application of CE/PRONTO3D to penetration problems, Brad Altman for developing the finite element model of the penetrator, Mike Forrestal for information on penetration modeling and experiments, Ned Hansen for penetration field test information and project management, Don McCoy for helpful discussions on modeling goals and project support, and Kevin Eklund for penetrator structural information and field test observations.

Introduction

Methods of understanding and predicting penetration into concrete and geologic targets can be classified as empirical, approximate engineering, or detailed numerical and may focus on trajectories, penetrator structural response, or the shock environment experienced by penetrator components. Empirical approaches may require extensive data bases, while the detailed numerical approaches, which couple an Eulerian target representation to a Lagrangian penetrator description, may be limited in scope or require long computer processing time. Approximate engineering models based on cavity expansion (CE) loading for normal penetration with two-dimensional motion were developed in Ref. [1] using cylindrical cavity expansion in a Mohr-Coulomb target and in Ref. [2] using spherical cavity expansion in concrete. Cavity expansion load modeling was extended to three-dimensional oblique penetration and coupled to an ABAQUS, Ref. [3], structural model of the penetrator for correlations with field tests into a soft rock and a soil in Refs. [4,5], respectively. In Ref. [6], a spherical cavity expansion loading option for penetration was implemented into PRONTO 3D, Ref. [7]. Ref. [8] correlates spherical cavity expansion loading with target near-surface effects and layering applied to an ABAQUS penetrator model with rock and frozen soil field test results.

In the present work, the spherical cavity expansion loading option of Ref. [6] is extended to account for relief of the penetrator loading caused by a nearby target free surface. The free-surface influence distance is determined in a predictive manner by considering the pressure to continuously expand a spherical cavity in a finite radius sphere of the target material. This development was required to obtain sufficient penetrator rotation in the process of correlating a penetration simulation with two, nearly identical, field tests of penetrators impacting frozen soil at an angle of 49 degrees from the horizontal. Parallel work is in progress, The present CE/PRONTO 3D penetration simulation procedure is evaluated by comparing the simulation results with the field test data. Measured penetration rotations were 24 and 22 degrees and the simulation, Fig. 1, gave a rotation of 21 degrees. Similar good agreement was found for the penetration depth and axial and lateral acceleration histories at two locations in the penetrators. Since the CE/PRONTO 3D approach can provide reasonable accuracy in predicting the penetrator trajectory and response, including shock environment and structural failure, and requires relatively short cpu time, it is suitable for use in a simulation-based penetrator design process.

Penetrator Structural Model

The PRONTO 3D model of the penetrator is shown in Fig. 1. The model consists of 12,028 hexahedral, 8-node elements. It has substantial detail since the goal of the simulation is to represent not only the penetrator trajectory but also the response of the on-board accelerometers, Fig. 1, and possible permanent structural deformation and failure. The tail is shortened by 18 inches from the length of the tail section in the actual penetrator before impact. This was done to account for the crushing of the forward portion of the tail between the preflight and the area of the fins, which was observed on recovery of penetrators in the field tests being simulated. The tail shell was thickened so that the mass is the same as that of its original length. Before crushing, the cap ballast was located at the interface of the tube ballast and aft ballast. The crushing results

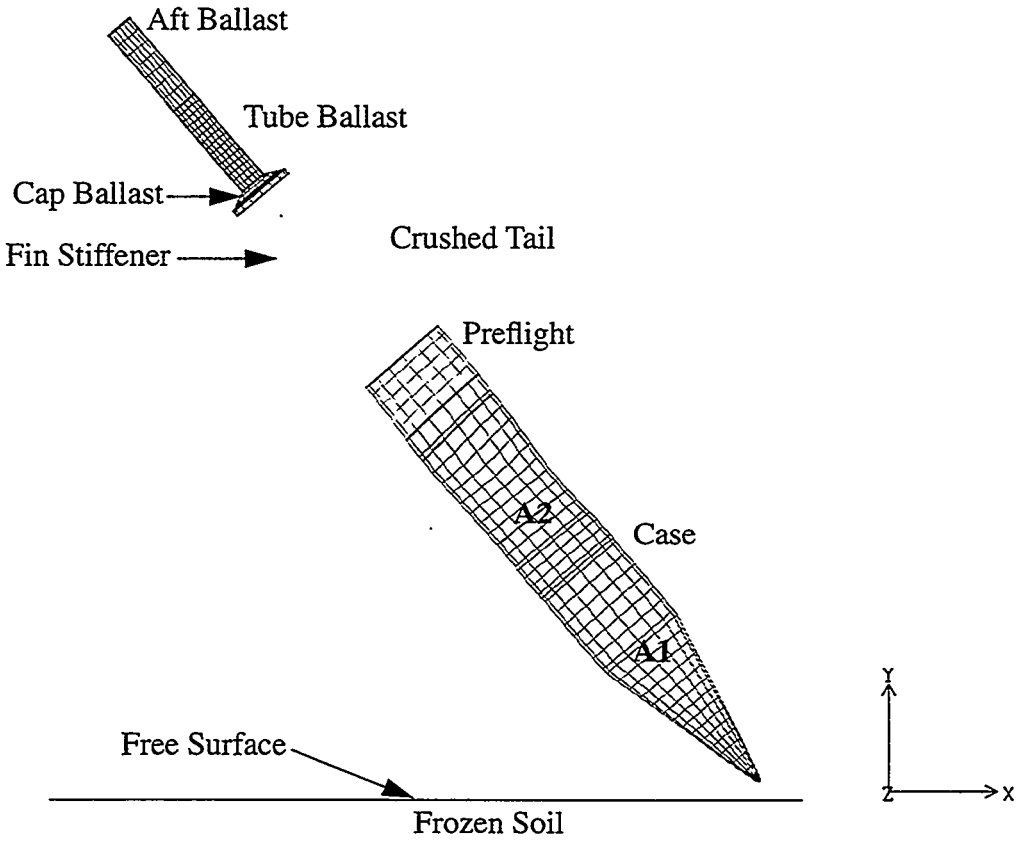

Fig. 1 Penetrator model and frozen soil target.

from the inertia load of the cap ballast which is only weakly connected to the aft ballast and slides along the ballast tube.

Another deviation concerns the four fins in the actual penetrator, which are spaced at 90 degree intervals and attached to the outside of the tail starting at the cap ballast. During the field tests the fins mostly remained attached. In the model the fins are replaced by stiffeners of equivalent bending stiffness and mass, equivalenced to the inside of the tail shell. This simplified the application of the cavity expansion loading to the penetrator.

A conical flare that surrounds the aft ballast in the actual penetrator is omitted in the model. This was done because the flare is relatively light, weakly attached to the penetrator, and was found separated from the penetrator on the surface of the frozen soil in the tests.

The material properties of the structural components of penetrator model are given in Table 1. All of the aluminum and steel components are elastic-plastic with isotropic strain hardening, except the fin stiffeners, which are elastic. In the tests considered herein, moderate permanent axial bending deformation and other deformation was visible. The densities of the preflight and fin materials are chosen to account for the actual mass of these components.

Table 1: Material properties of penetrator components.

Compo-nent	Material	Density (lb-s^2-in.^{4})	Model	Young's Modulus (psi)	Poisson's Ratio	Yield Stress (psi)	Hard. Modulus (psi)
nose/case	steel	7.32e-4	el-pl	30.e+6	0.30	1.82e+5	1.04e+5
preflight	alum.	7.70e-4	el-pl	10.2e+6	0.33	5.90e+4	1.35e+5
tube bal.	"	7.50e-4	"	29.4e+6	0.28	1.66e+5	1.55e+5
cap bal.	"	7.57e-4	"	28.0e+6	0.28	3.6e+4	7.16e+4
aft bal.	"	7.50e-4	"	"	"	"	"
tail	alum.	2.53e-4	"	10.e+6	0.33	4.0e+4	4.3e+4
fins	equiv.	1.08e-4	elastic	227.e+6	0.33	-	-

The inertia properties of the model closely approximate those of the actual penetrator. The mass, moment of inertia in the z direction at the center of mass, and location of the center of mass relative to the tip of an uncrushed model consistent with the crushed-tail model are within 1% of the actual penetrator design definition. In the uncrushed model the shortened tail of the crushed model is replaced by one of the original length and the mass of the flare is added to the aft ballast. In the crushed model, the center of mass is shifted forward about 5% of the distance to the tip and the moment of inertia is reduced 19% relative to the pre-impact configuration.

Cavity Expansion Loading with Target Free-Surface Effects

The loading on the penetrator is not determined from the response of a 3-D discretized model of the frozen soil target, but rather from the solution of a 1-D related problem, that of an expanding spherical cavity in an infinite medium of the frozen soil, adjusted to account for the target free surface. The applied pressure at a penetrator surface node is specified as the pressure to expand the spherical cavity with a radial expansion velocity equal to the nodal velocity component normal to the penetrator surface, Fig. 2. These pressures at the verticies of an element side are averaged to specify the pressure acting on an element side of the penetrator surface, as implemented in Ref. [6].

The expansion of a spherical cavity in an infinite medium of the target material produces regions of plastic, cracked, and elastic response, as indicated in Fig. 3. The features of the material response are the same as in Ref. [2]. Material compressibility is modeled by a linear pressure-volume strain relation with bulk modulus K. In the plastic region, shear strength is represented by a Mohr-Coulomb failure criterion with parameters, λ, which defines the linear dependence on pressure, and Y, which is the unconfined compressive strength. In the radially cracked region, the tangential stress is zero, representing material that has failed in tension, as a result of the tensile strength, T, being significantly smaller than Y. Tangential tensile stress in the

elastic region is less than T and the response is defined by Young's modulus, $E = 3K(1-2\nu)$, and Poisson's ratio, ν.

As in Ref. [2], the mass and momentum conservation laws can be applied using the geometry of Fig. 3 and the material response described above to develop a set of 1-D nonlinear differential equations for the target response to an expanding spherical cavity. For a given value of radial expansion velocity $\dot{a}$ these may be solved by standard numerical techniques to determine the corresponding expansion pressure P. A set of these values was calculated, Fig. 4, for the following parameter values, representative of frozen soil: ρ_0=1.93x10^{-4} lb-s^2/in.^{4}, K=4.96x10^5 psi, Y=1,300 psi, λ=0, T=107 psi, and ν=0.27. There is a substantial uncertainity in the properties of frozen soil, as indicated in Ref. [9], and the strength values used fall near the low end of the range. Also shown in Fig. 4 is the quadratic fit to the spherical cavity expansion (SCE) solution,

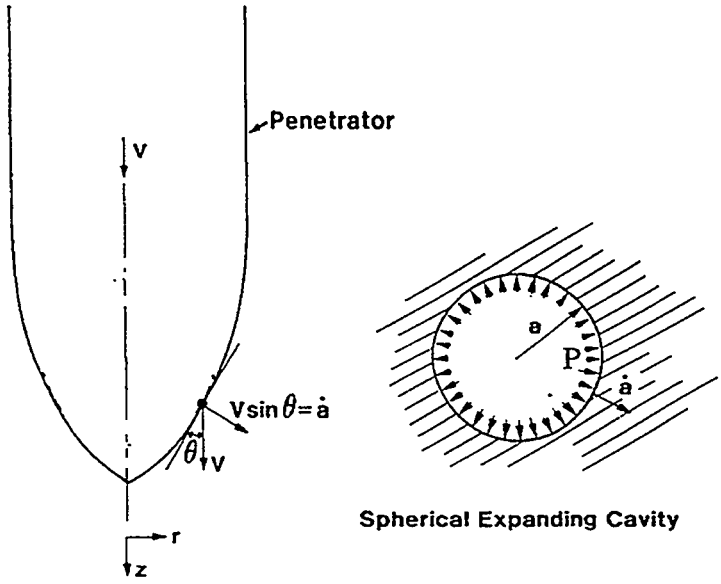

Fig. 2 Relation of penetrator motion to spherical cavity expansion.

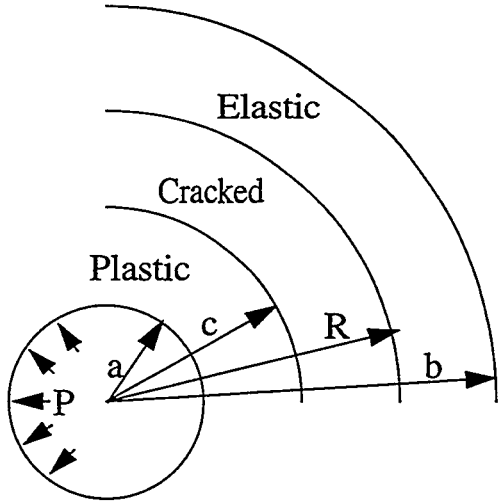

Fig. 3. Target response regions.

the coefficients of which are input to specify the cavity expansion loading option in PRONTO 3D.

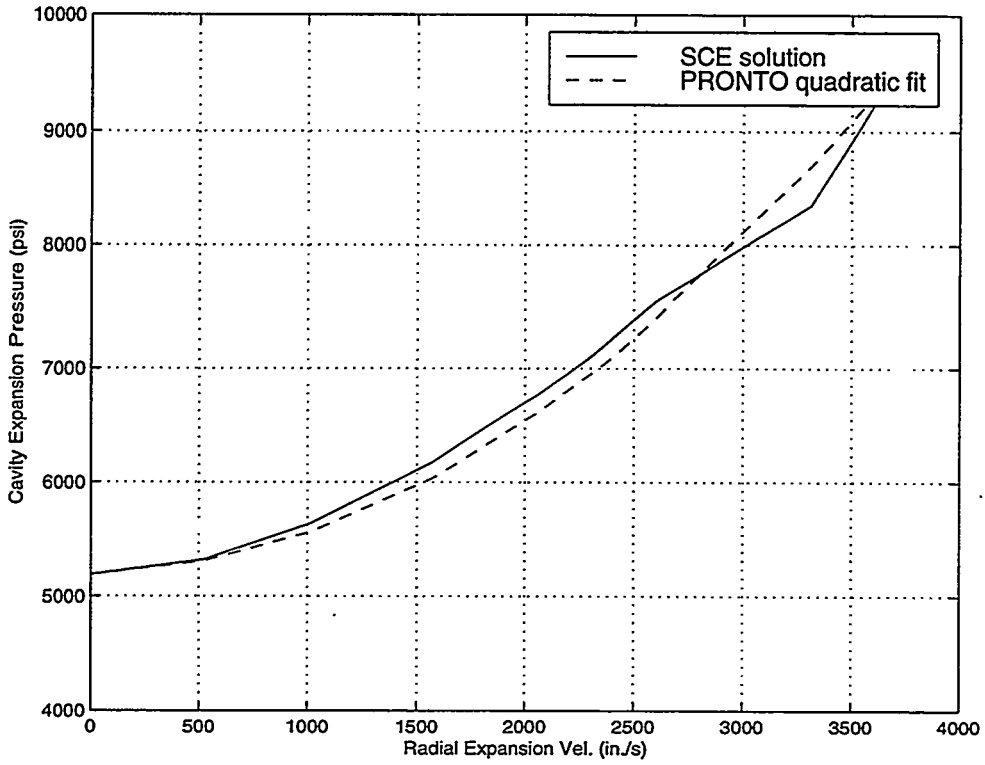

Fig. 4 Spherical cavity expansion pressure-velocity for frozen soil

The only effect of the target free surface on the cavity expansion loading, as originally implemented in PRONTO 3D, Ref. [6], is from the nonsymmetrical contact of the target on the penetrator during the oblique entry shown in Fig. 1. As discussed later, this model produced an insignificant penetrator rotation compared with the rotations measued in the field tests.

As the penetrator progresses into the target it should be easier to push aside material in the direction of the nearby free surface than in the opposite direction. The difficulty in expanding a cavity should depend on the distance to the free surface and on the size of the cavity being created. This is modeled by requiring the loading on the penetrator to depend on the nondimensional distance to the free surface, d/a, as indicated in Fig. 5. The distance d is taken from a surface node to the free surface along a normal to the penetrator surface and a is a radius, characteristic of the local penetrator geometry, at the node. The pressure loading on the penetrator is reduced to zero when d/a is less than a critical value $(d/a)^*$ and is the full cavity expansion pressure when d/a is greater than $(d/a)^*$. This is represented by

$$P_L = \begin{cases} 0, & d/a < (d/a)^* \\ P, & d/a > (d/a)^* \end{cases}$$

where P_L is the pressure loading applied to the penetrator model and P is the cavity expansion pressure in an infinite medium. This procedure for modeling the free surface effect on penetrator

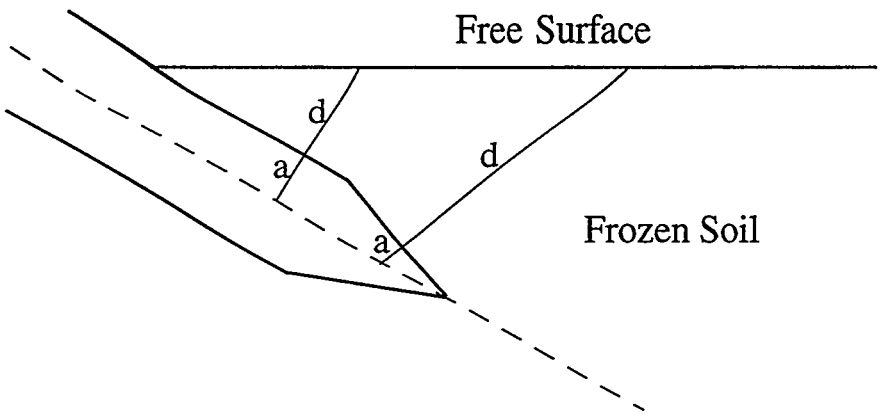

Fig. 5 Geometry of free surface effect model

loading has been implemented into the cavity expansion loading option in PRONTO 3D. The value $(d/a)^*$ can be chosen empirically to best fit available data or can be estimated in a predictive manner by considering the expansion of a spherical cavity in a finite radius sphere of the target material.

For the purpose of calculating a value of $(d/a)^*$, the same response regions and geometry of Fig. 3 apply except that now b is the radius of the outer, assumed free, surface of the finite sphere and the response is assumed to be quasistatic, which is satisfied by the field test impact conditions. Under the additional assumptions of constant yield strength in the plastic region and incompressible material response, a solution is developed in the APPENDIX for the pressure P to expand a spherical cavity to any radius a in a finite sphere. The procedure is similar to that in Ref. [10] for a finite elastic-plastic sphere and uses some steps from the analysis of an infinite, elastic-cracked-plastic medium in Ref. [11]. Results of the solution, for the frozen soil parameter values given previously, are shown in Fig. 6. The pressure is constant for large b/a, which correspondes to expansion in an infinite medium, and then decreases rapidly as the cavity radius a becomes large enough to be influenced by the free surface at radius b. A closed-form expression for the zero-pressure asymptote has the value of b/a=16.2 in Fig. 6. This asymptote provides an estimate of the critical nondimensional free surface distance within which the penetrator loading of our model is set to zero. The relatively sharp drop-off to zero of the pressure in Fig. 6 justifies our model in which the pressure on the penetrator is either the full cavity expansion pressure in an infinite medium or zero. This behavior is related to the region of tensile fracturing response in Fig. 3, which is significant because the tensile strength is an order of magnitude lower than the compressive yield strength, as is characteristic of concrete, rock, and ice.

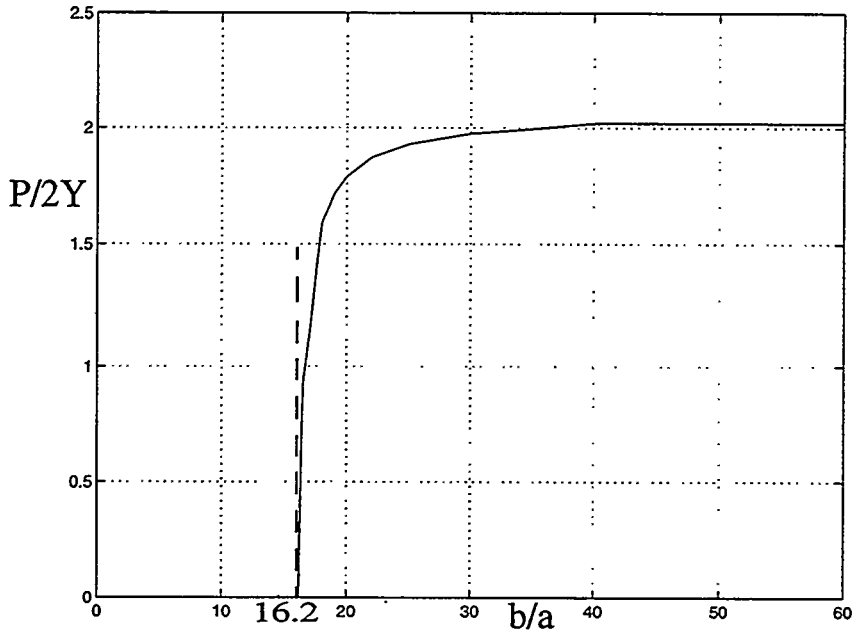

Fig. 6 SCE pressure in a finite sphere of frozen soil.

Simulation Results

The simulation represents the conditions of Test No. 4 in which a full-scale penetrator was air-dropped into frozen soil in Alaska. The impact conditions were a velocity of 718 f/s, a 49.6 degree impact angle (Fig. 1), and a zero angle of attack. The impact angle is the angle between the velocity vector and the horizontal and the angle of attack is the angle between the velocity vector and the penetrator axis. The impact conditions were not directly measured, but were inferred from an aerodynamic simulation, Ref. [12]. With the penetrator model of Fig. 1, the frozen soil cavity expansion loading of Fig. 4, and a surface effect parameter value $(d/a)^*$=15.6, a solution for the penetrator motion over its full trajectory was obtained using the PRONTO 3D explicit solution procedure in approximately 12 hours on a Sun Ultra 2 workstation (300 MHz). value of $(d/a)^*$ was adjusted slightly from the initially calculated value of 16.2 to provide a little better correlation with the test results. With a conical-nose half angle of 13.4 degrees and impact velocity of 718 f/s the maximum cavity expansion velocity required for the penetrator loading is 2,000 in./s, which (with Fig. 4) shows dynamic effects are fairly small and justifies use of the quasistatic approximation in calculating $((d/a)^*$.

The penetrator impact and calculated final positions and the calculated penetrator rotation at the forward accelerometer (A1 in Fig. 1) are shown in Figs. 7 and 8, respectively. Some permanent bending of the tail shell and the tube ballast is indicated. The calculated final penetrator rotation is 21 degrees and the measured rotation is 24 degrees in Test No. 4. Another simulation, identical to the first but with no free surface effects, $(d/a)^*$=0, gave a nearly straight trajectory with a final penetrator rotation of 2 degrees. A comparison of penetration trajectory results of the simulation with Test No. 4 and Test No. 18, which had nearly identical impact conditions (veloc-

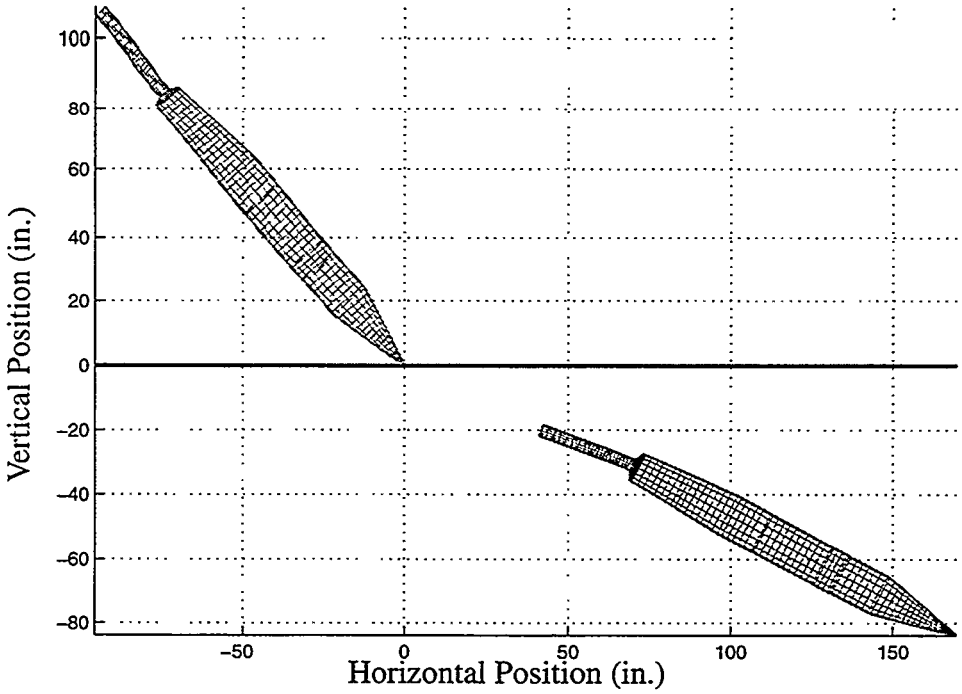

Fig. 7 Penetrator initial and final positions.

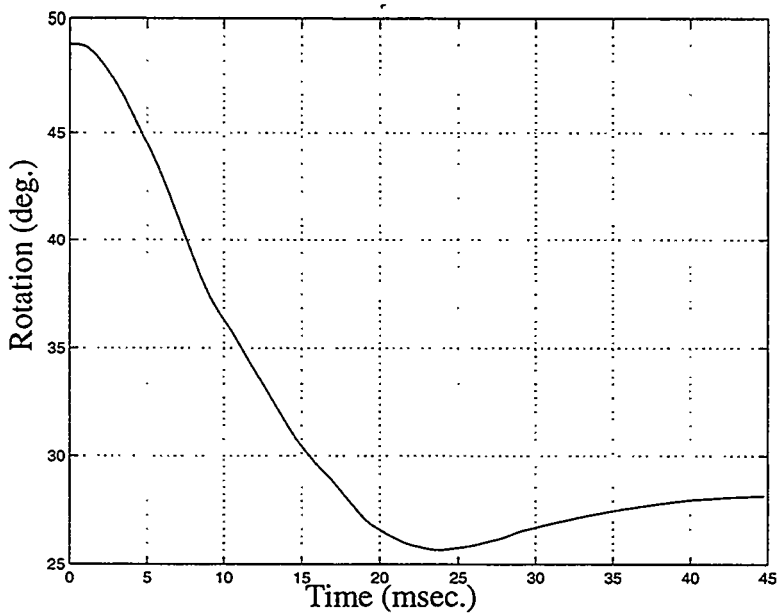

Fig. 8 Penetrator rotation.

ity of 738 f/s and impact angle of 52.5 degrees) is shown in Table 2. The distance is along a

Table 2: Penetration trajectory results for simulation and tests

Source	Rotation (deg.)	Depth (ft.)	Distance (ft.)
Test No. 4	24	9.4	15.8
Test No. 18	22	8.3	15.7
Simulation	21	7.0	15.4

straight line from the initial to final tip positions.

In Test No. 4, triaxial accelerometers at locations A1 and A2 in Fig. 1 measured the axial and two perpendicular components of lateral acceleration. These accelerations were calculated in the simulation and compared with the data in Figs. 9-12. Both the calculated and measured accelerations were filtered analytically with a 4-pole, Butterworth, low-pass filter with a 500 Hz cutoff frequency, available in MATLAB, Ref. [13]. The axial acceleration data is consistent at the two stations and the calculations agree with the peaks and rise times of the data, but do not decrease as rapidly as the measurements. The lateral accelerations are compared as the vector magnitude of the components and show more deviation of the analysis and data, but good agreement in the

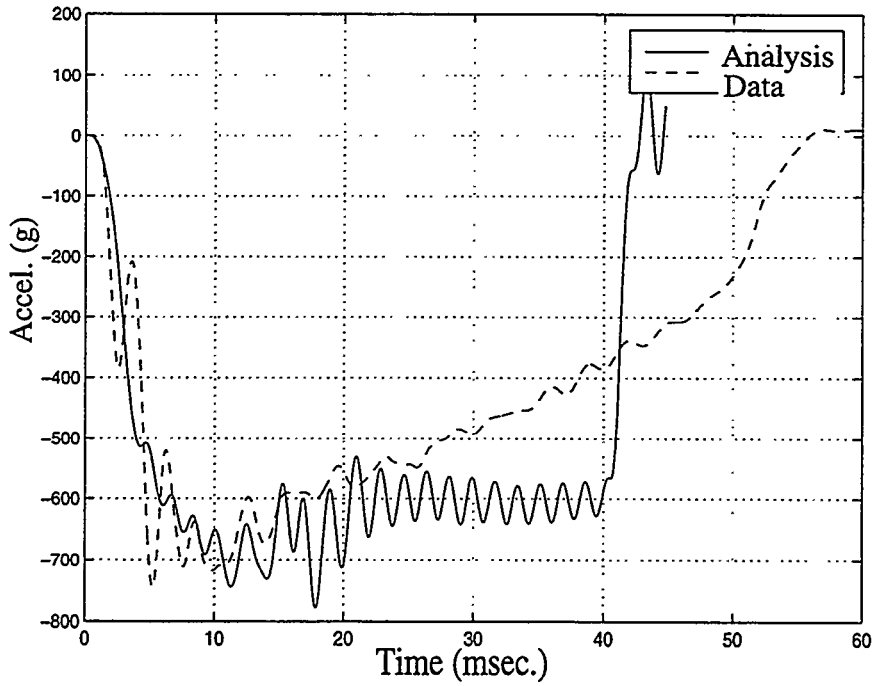

Fig. 9 Axial acceleration at A1.

peaks and durations. Generally, the agreement is good considering the uncertainities in impact conditions and frozen soil composition.

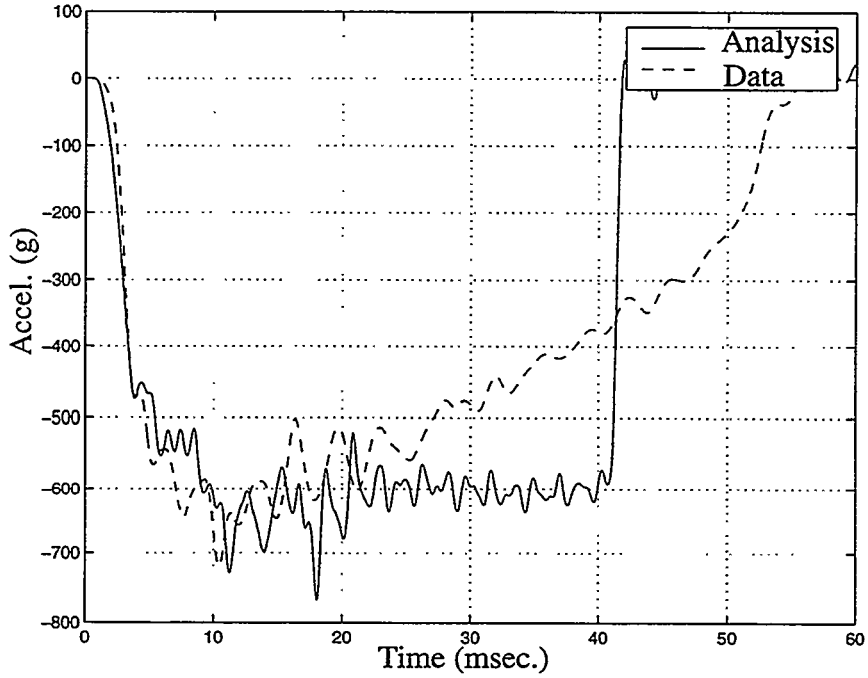

Fig. 10 Axial acceleration at A2

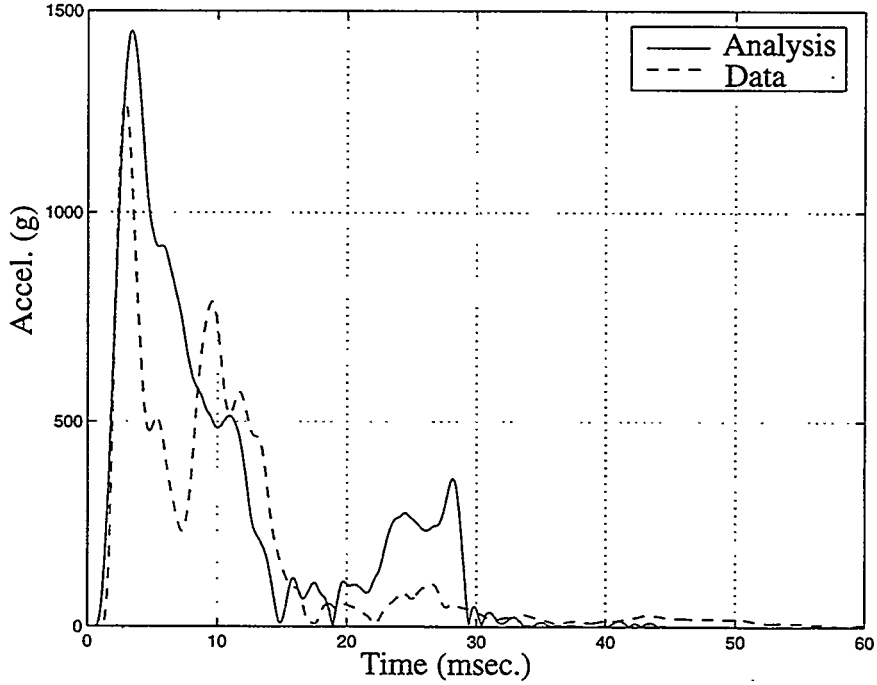

Fig. 11 Lateral acceleration magnitude at A1.

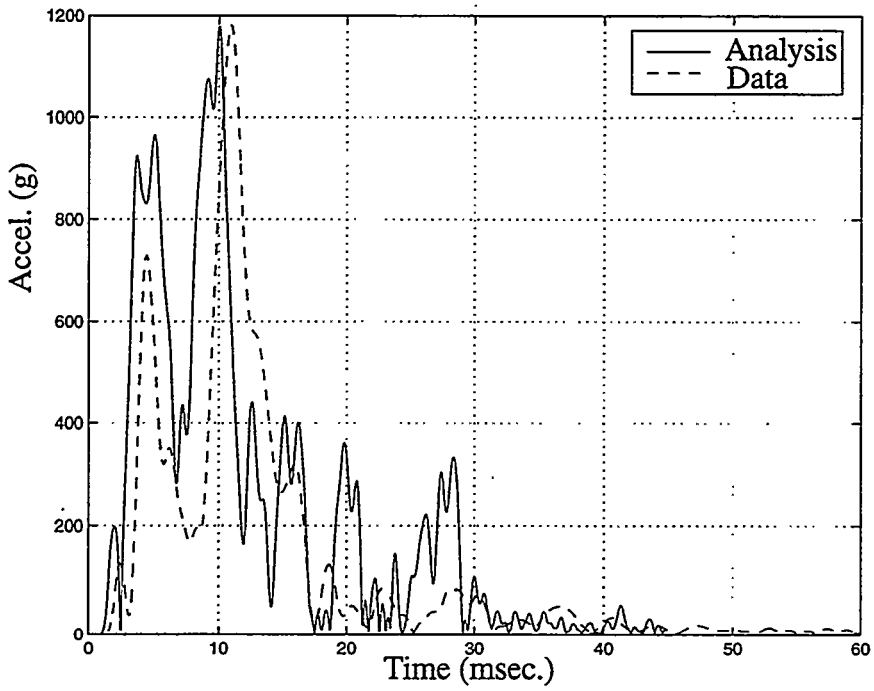

Fig. 12 Lateral acceleration magnitude at A2.

Conclusion

A new procedure has been developed and implemented into PRONTO 3D for cavity expansion based penetrator loading during oblique impact that accounts for the pressure relief from a nearby target free surface. This procedure has been evaluated by comparing its results with data on penetration depth, penetrator rotation, and axial and lateral acceleration from two full-scale field tests into Alaskan frozen soil and good agreement was demonstrated. We found the inclusion of free-surface pressure relief in the lateral loading was essential to obtain sufficient penetrator rotation and lateral acceleration magnitude and representing the very low tensile strength of the frozen soil was important to the surface effect. Although the comparisons provide some validation of this procedure as a predictive tool, this conclusion is tentative because of the substantial uncertainity in the frozen soil material properties. Since the CE/PRONTO 3D approach can provide reasonable accuracy in predicting the penetrator trajectory and structural response, and requires relatively short cpu time, it is suitable for use in a simulation-based penetrator design process.

References

1. Longcope, D. B. and Forrestal, M. J., "Penetration of Targets Described by a Mohr-Coulomb Failure Criterion with a Tension Cutoff," Journal of Applied Mechanics, Vol. 50, June, 1983, pp 327-333.

2. Forrestal, M. J. and Tzou, D. Y., "A Spherical Cavity-Expansion Penetration Model for Concrete Targets," Int. J. Solids Structures Vol. 34, Nos. 31-32, pp. 4127-4146, 1997.
3. ABAQUS/Standard User's Manual, Version 5.5, Vols. I and II, Hibbet, Karlson, Sorensen, Inc., Providence, RI, 1995.
4. Longcope, D. B., "Coupled Bending / Lateral Load Modeling of Earth Penetrators," SAND-0789, Sandia National Laboratories, Albuquerque, NM, June, 1991.
5. Longcope, D. B. "Oblique Penetration Modeling and Correlation with Field Tests into a Soil Target," SAND96-2239, Sandia National Laboratories, Albuquerque, NM, Sept. 1996.
6. Warren, T. L. and Tabbara, M. R., "Spherical Cavity-Expansion Forcing Function in PRONTO 3D for Application to Penetration Problems," SAND97-1174, Sandia National Laboratories, Albuquerque, NM, May, 1997.
7. Taylor, L.M. and Flanagan, D.P., "PRONTO 3D a Three-dimensional Transient Solid Dynamics Program," SAND87-1912, Sandia National Laboratories, Albuquerque, NM, 1989.
8. Macek, R. W. and Duffey, T. A., Finite Cavity Expansion Method for Near-Surface Effects and Layering During Earth Penetration, I.C.I.S. 98 Conference Proceedings, Modeling and Simulation Based Engineering, Vol. II, Tech Science Press, Palmdale, CA, 1998, pp. 1138-1143.
9. Furnish, Michael D., "Measuring Static and Dynamic Properties of Frozen Silty Soils," SAND98-1497, Sandia National Laboratories, Albuquerque, NM, Sept., 1998.
10. Johnson, W. and Mellor, P. B., Engineering Plasticity, Van Nostrand Reinhold, London, 1973.
11. Forrestal, M.J. and Longcope, D.B., "Target Strength of Ceramic Materials for High-Velocity Penetration," J. Appl. Phys., Vol. 67, No. 8, April 15, 1990.
12. Chavez, Ken, private communication, Dept. 9115, Sandia National Laboratories, Albuquerque, NM, 1998.
13. Little, J. N. and Shure, L., "Signal Processing Toolbox for Use with MATLAB," The Math Works, Inc., Natick, Mass., July, 1992.

Appendix

We develop the relation between pressure P and radius a of a spherical cavity expanding quasistatically in a finite sphere of the target material, Fig. 3. The outer surface of the sphere at Eulerian radius $r = b$ is assumed free. We assume the tensile strength T is less than the unconfined compressive yield strength Y, so the sphere will have the plastic, cracked, and elastic response regions shown. If $T > Y$, the response will only have elastic and plastic regions, Ref. [10]. In the plastic region, the equilibrium equation is

$$\frac{d\sigma_r}{dr} + \frac{2(\sigma_r - \sigma_\theta)}{r} = 0, \tag{1}$$

where r is the Eulerian radial coordinate and σ_r and σ_θ are the radial and tangential Cauchy stresses, respectively. The failure criterion in the plastic region is

$$\sigma_r - \sigma_\theta = Y, \tag{2}$$

which represents the constant strength limiting case of a Mohr-Coulomb criterion. In the cracked region, $\sigma_\theta = 0$ throughout and the equilibrium equation is (1) with $\sigma_\theta = 0$. Solving the equilibrium equations in the plastic and cracked regions gives $\sigma_r = A - 2Y\ln r$ and $\sigma_r = Br^{-2}$, respectively, where A, B are integration constants. Applying $\sigma_r(a) = P$ and continuity of σ_r and incipient failure at $r = c$ to the solutions gives

$$P = Y + 2Y\ln\left(\frac{c}{a}\right), \tag{3}$$

where c/a is unknown at this point. In the elastic region, the well-known solution, which satisfies $\sigma_\theta = -T$ at $r = R$ (location of maximum tensile stress) is

$$\sigma_r = T\left[\frac{b^3/r^3 - 1}{b^3/(2R^3) + 1}\right], \tag{4a}$$

$$\sigma_\theta = -T\left[\frac{b^3/(2r^3) + 1}{b^3/(2R^3) + 1}\right], \tag{4b}$$

$$u_r = \frac{T}{E}\left[\frac{(1-2\nu)r + (1+\nu)b^2/(2r^2)}{b^3/(2R^3) + 1}\right], \tag{4c}$$

Applying continuity of σ_r at $r = R$ gives

$$\frac{c^2}{R^2} = \frac{T}{Y}\left[\frac{b^3/R^3 - 1}{b^3/(2R^3) + 1}\right], \tag{5}$$

Applying conservation of mass

$$R_0^2 - a_0^2 = R^2 - a^2 \ , \tag{6}$$

where a_0 is the initial hole radius and $R_0 = R - u_r$ is the initial radius of the particle currently at R. We substitute for R_0 in Eq. (6) using Eq. (4c) with $\nu = 1/2$ (assuming incompressibility) and take the limit as $a_0/a \to 0$ (a_0 can be arbitrarily small compared to a) to give

$$R/a = [\varepsilon - 2(a/b)^3]^{-1/3}, \varepsilon = \frac{9T}{2E} \ , \tag{7}$$

We imagine a displacement controlled process of increasing the cavity radius a, by, say, injecting an incompressible fluid into the cavity, and determining the corresponding pressure until a approaches b and the pressure P drops to zero. This is analagous to the penetration process in which a cavity is created in the target by the penetrator. To calculate P, we assume a value of a/b; use Eq. (7) to calculate R/a; with $(b/R) = (b/a)(a/R)$, use Eq. (5) to determine c/R; and with $c/a=(c/R)(R/a)$, use Eq. (3) to determine P. From Eq. (3), this procedure is valid for $P > Y$. The solution sequence starts with a large value of b/a and as b/a decreases P is approximately constant. This corresponds to the expansion of a cavity whose radius is small compared to the outer, free surface radius and is the limiting case of cavity expansion in an infinite medium. As b/a becomes small enough, P begins to decrease and the plastic region shrinks while the cracked region increases in size. When $c = a$ the plastic region disappears and $P = Y$.

For $P < Y$, there are only two response regions, cracked and elastic. Using a procedure similar to that discussed previously, we determine the pressure to be

$$P = \frac{T(R^2/a^2)(b^3/R^3 - 1)}{b^3/(2R^3) + 1} \ , \tag{8}$$

As before, using conservation of mass and incompressibility, we determine that Eq. (7) continues to hold for $P < Y$. By Eq. (8), when the cracked boundary reaches the outer radius, $R = b$, the pressure P becomes zero. Substituting $R = b$ in Eq. (7), we solve for b/a

$$(b/a)^* = (3/\varepsilon)^{1/3}, \tag{9}$$

This is the value of b/a at which P becomes zero and we take this to be the critical value $(d/a)^*$ at which the pressure applied to the penetrator changes from the cavity expansion pressure in an infinite medium to zero. The curve of Fig. 6 and the zero-pressure value, b/a =16.2, were computed using the previously specified parameter values Y = 1,300 psi, T = 107 psi, and $E = 6.85\text{x}10^5$psi (from $K = 4.96\text{x}10^5$ psi and $\nu = 0.27$) and the procedure given above.

$$(d/a)^* = (3/\varepsilon)^{1/3}, \tag{10}$$

Distribution:

(2) Applied Research Associates, Inc.
Attn: Wayne Young
Peter Dunn
4300 San Mateo Boulevard NE
Suite A220
Albuquerque, NM 87110

(1) HQ/DNA/SPSD
Defense Nuclear Agency
Attn: Mike Giltrud
6801 Telegraph Road
Alexandria, VA 22310-3398

(1) Lawrence Livermore National Laboratory
Attn: Francois Heuze
P. O. Box 808, L-200
Livermore, CA 94550

(1) Lawrence Livermore National Laboratory
Attn: Albert Holt
P. O. Box 808, L-163
Livermore, CA 94550

(2) Los Alamos National Laboratory
Attn: Richard Macek
Thomas Duffey
Group ESA-EA, MS-0807
Los Alamos, NM 87544

(2) Waterways Experiment Station
Geomechanics and Explosion Effects
Attn: Mark Adley
J. Donald Cargile
3909 Halls Ferry Road
Vicksburg, MS 39180-6199

(1) Wright Lab Armament Directorate
WL/MNMW
Attn: Dr. Joseph Foster, Jr.
101 W. Eglin Boulevard, Ste. 239
Eglin AFB, FL 32542-6810